Received 10 May 2009
Revised 20 August 2009
Accepted 10 September 2009

Numerical study of buoyancy-driven transitional flow in a square cavity with partially heated and cooled vertical walls

Rangaswamy Navamani
Department of Mathematics, Coimbatore Institute of Technology, Coimbatore, India, and
Nadarajan Murugan
Department of Mechanical Engineering, Coimbatore Institute of Technology, Coimbatore, India

Abstract

Purpose – The purpose of this paper is to numerically study transient natural convective flow in a square cavity with partially heated and cooled vertical walls, thermally insulated top wall and linearly heated bottom wall.

Design/methodology/approach – The governing equations of motion are non-dimensionalized and reformulated using stream function-vorticity approach. Alternating direction implicit finite difference scheme is used to solve the coupled equations.

Findings – The transient results obtained for different values of Grashof number (Gr) and fixed Prandtl number $Pr = 0.733$ are presented in the form of isotherms, streamlines, bifurcation diagram and time series. The transition from steady to oscillatory motions is analyzed in detail with respect to Gr. The flow is observed to be steady up to $Gr \approx 2 \times 10^4$. A time-periodic unsteady solution first appears at $Gr = 20{,}900$ and the amplitude of the fluctuation grows as Gr is increased.

Research limitations/implications – The study is limited to laminar flow in a square cavity. Further extension of this work could include the influence of various choices of Prandtl number and the effect of aspect ratio. Buoyancy-driven convection in a sealed cavity with differentially heated walls is a prototype of many industrial applications such as energy-efficient design of buildings and rooms, convective heat transfer associated with boilers, etc.

Originality/value – The paper presents an original computer program written in FORTRAN to solve the partial differential equations.

Keywords Convection, Vortices, Time series analysis, Laminar flow
Paper type Research paper

Nomenclature

C_P	specific heat
Gr	Grashof number
g	acceleration due to gravity
l	side of the enclosure
Nu	Nusselt number
$\overline{Nu}$	average Nusselt number
p'	pressure
Pr	Prandtl number
t	time
u	velocity along x direction
v	velocity along y direction

Dimensionless variables

P	fluid pressure
T	temperature
U	velocity along X direction
V	velocity along Y direction
X	distance along x-coordinate

International Journal of Numerical Methods for Heat & Fluid Flow
Vol. 20 No. 7, 2010
pp. 744-758

0961-5539
DOI 10.1108/09615531011065548

Y distance along y-coordinate

Greek symbols

β volume expansion coefficient

θ_0 initial temperature

θ_h temperature along the hot wall

θ_c temperature along the cold wall

ζ dimensionless vorticity

μ viscosity

ν kinematic viscosity

ρ density

τ dimensionless time

ψ stream function

1. Introduction

The convective motion driven by the buoyancy forces is a well-known natural phenomenon and has attracted interest of many researchers. In particular, the topic of natural convection in cavities has received much attention in the past since many practical heat transfer situations can be modeled as flows in cavities.

There have been numerous investigations of natural convective heat transfer that occurs in an enclosure (Sathiyamoorthy *et al.*, 2007; Marcello and Milanez, 1995; Wright *et al.*, 2005; Wu *et al.*, 2005; Yang, 1988; Newell and Schmidt, 1970; Valencia and Fredrick, 1989; Kandaswamy and Nithyadevi, 2007). Sathiyamoorthy *et al.* (2007) presented the numerical study of steady natural convection in a closed square cavity under different boundary conditions. They analyzed the influence of heated vertical walls on the flow and heat transfer characteristics when the bottom wall was uniformly and non-uniformly heated and top wall was thermally insulated. They showed that for small Rayleigh numbers (*Ra*), the average Nusselt number was almost constant due to heat conduction and increased steadily as *Ra* increased.

Marcello and Milanez (1995) analyzed the steady natural convection in an enclosure which was heated from below and symmetrically cooled from the sides. The results discussed for wide range of parameters like Prandtl number (*Pr*), Rayleigh number (*Ra*) and aspect ratio showed that on the Nusselt number, the influence of *Pr* was less compared to other parameters. Wright *et al.* (2005) depicted the flow visualization of natural convection in a tall, air-filled vertical cavity based on the experimental study for the aspect ratio 40. The flow was found to be stable for $Ra < 10^4$ and irregular for higher Ra. Most of the temperature drop existed in boundary layers near the walls.

Wu *et al.* (2005) studied experimentally the effect of the top and bottom wall temperatures on the heat transfer characteristics in an air-filled square cavity driven by difference in the vertical wall temperatures. They observed that changes in the top and bottom wall temperatures changed the temperature gradient and the average temperature of the air outside the thermal boundary layers in the cavity. Yang (1988) reviewed the experimental and numerical studies of flow instability, bifurcation and transition to turbulence for buoyant flow in three-dimensional rectangular enclosures heated from below and from the sides, with emphasis on the routes to chaotic motion in detail.

Newell and Schmidt (1970) presented the time dependent two-dimensional natural convection of air in a long horizontal enclosure with isothermal walls kept at different temperatures using Crank and Nicholson method. The same problem was discussed by Valencia and Fredrick (1989) with half active and half insulated vertical walls.

Kandaswamy and Nithyadevi (2007) numerically analyzed the buoyancy-driven convection of water near its density maximum with partially active vertical walls in a square cavity. They observed that the average Nusselt number behaved nonlinearly as a function of *Gr* and the heat transfer rate decreased in the density maximum regions. Basak *et al.* (2006) studied the steady effect of continuous and discontinuous Dirichlet

boundary conditions on the flow and heat transfer characteristics due to natural convection within a square enclosure. They reported that non-uniform heating of the bottom wall produced greater heat transfer rates at the center of the bottom wall than the uniform heating case for all *Ra*.

From the above-mentioned studies, it could be observed that the buoyancy-induced flows in cavities with differentially heated bottom, top or side walls, display a circular motion inside the cavity. Near the heated vertical surface, the fluid has a tendency to rise and the cooler fluid shows a tendency to flow in the opposite direction. When the two vertical walls of a cavity are differentially heated with top and bottom walls adiabatic, due to the temperature difference, fluid flow occurs inside the enclosure. Also, when the temperature difference quotient is horizontal and perpendicular to the gravity vector, direction of the circulation is observed to depend on their orientation. In cavities with either the top or bottom surface heated, the formation of counter rotating cells has been noted. From the literature survey it is inferred that walls of the enclosures are either heated or cooled uniformly in the vertical direction. Very less attention has been given to the unsteady natural convection with simultaneous partial heating and cooling of vertical walls.

In the present study, thus, an unsteady natural convection problem in a square enclosure with partially heated and cooled vertical walls is being analyzed numerically. It is assumed that the heated and cooled surface elements face each other in an opposed manner. The bottom wall is assumed to be linearly heated and the top wall is thermally insulated.

Mathematical formulation of the problem is presented and the equations of mass, momentum and energy for the flow inside a square cavity are detailed. The governing equations are transformed to non-dimensional form and solved by finite-difference method. To support the current numerical calculations corroborative evidence is provided in the results and discussion section. Emphasis has been placed on the influence of the dimensionless Grashof number on the flow field variables and heat transfer coefficient. Numerical predictions of flow streamlines, isothermals are obtained for a wide range of Gr varying from 100 to 30,000 for a fixed $Pr = 0.733$.

2. Mathematical formulation

A square cavity of length, l filled with fluid (air) as shown in Figure 1 is considered in the present study. The fluid is assumed to be initially motionless and at a uniform temperature θ_0, which is equal to the average of the temperatures at the vertical walls.

Upper and lower half portions of the left vertical wall are assumed to be maintained at hot and cold temperatures, say, θ_h and θ_c, respectively, with $\theta_h > \theta_c$. The top wall is assumed to be thermally insulated and the bottom wall is maintained at a temperature $\theta = \theta_c + (\theta_h - \theta_c)\, y/\ell$. Temperature along the cold and hot portions on the right vertical wall are θ_c and θ_h, respectively. It is assumed that the effect of viscous dissipation is negligible in the energy equation. Under these assumptions, the equations of mass, momentum and energy with Boussinesq's approximation are as follows:

$$\frac{\partial u}{\partial x} + \frac{\partial v}{\partial y} = 0 \tag{1}$$

$$\frac{\partial u}{\partial t} + u\frac{\partial u}{\partial x} + v\frac{\partial u}{\partial y} = -g\beta(\theta - \theta_0) - \frac{1}{\rho}\frac{\partial p'}{\partial x} + \nu\left(\frac{\partial^2 u}{\partial x^2} + \frac{\partial^2 u}{\partial y^2}\right) \tag{2}$$

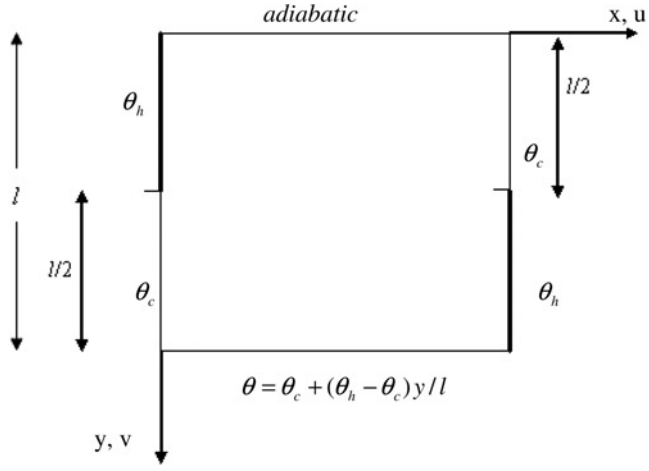

Figure 1.
Schematic of the square cavity

$$\frac{\partial v}{\partial t} + u\frac{\partial v}{\partial x} + v\frac{\partial v}{\partial y} = -\frac{1}{\rho}\frac{\partial p'}{\partial y} + \nu\left(\frac{\partial^2 v}{\partial x^2} + \frac{\partial^2 v}{\partial y^2}\right) \tag{3}$$

$$\frac{\partial \theta}{\partial t} + u\frac{\partial \theta}{\partial x} + v\frac{\partial \theta}{\partial y} = \frac{K}{\rho C_P}\left(\frac{\partial^2 \theta}{\partial x^2} + \frac{\partial^2 \theta}{\partial y^2}\right) \tag{4}$$

The initial and boundary conditions are given by:

$$\begin{aligned}
&t = 0{:}\ 0 \le x \le l, \quad 0 \le y \le l, \quad u = v = 0, \quad \theta = \theta_0 \\
&t > 0{:}\ x = 0; \quad u = v = 0;\ \frac{\partial \theta}{\partial x} = 0 \\
&\qquad x = l; \quad u = v = 0;\ \theta = \theta_c + (\theta_h - \theta_c) y/l \\
&\qquad y = 0; \quad u = v = 0;\ \theta = \begin{cases} \theta_h & 0 \le x \le l/2 \\ \theta_c & l/2 < x \le l \end{cases} \\
&\qquad y = l; \quad u = v = 0;\ \theta = \begin{cases} \theta_c & 0 \le x \le l/2 \\ \theta_h & l/2 < x \le l \end{cases}
\end{aligned} \tag{5}$$

By introducing the following dimensionless variables:

$$\begin{gathered}
X = \frac{x}{l}, Y = \frac{y}{l}, U = \frac{ul}{\gamma}, V = \frac{vl}{\gamma}, P = \frac{p \cdot l^2}{\rho\gamma^2}, T = \frac{\theta - \theta_0}{\theta_h - \theta_0}, \tau = \frac{t\gamma}{l^2} \\
Gr = \frac{g\beta(\theta_h - \theta_c)l^3}{\nu^2}, \mathrm{Pr} = \frac{\mu c_p}{k}
\end{gathered} \tag{6}$$

in the above equations (1)-(4), they are restated in the following dimensionless form as:

$$\frac{\partial U}{\partial X} + \frac{\partial V}{\partial Y} = 0 \tag{7}$$

$$\frac{\partial U}{\partial \tau}+U\frac{\partial U}{\partial X}+V\frac{\partial U}{\partial Y}=-\frac{Gr}{2}T-\frac{\partial P}{\partial X}+\frac{\partial^2 U}{\partial X^2}+\frac{\partial^2 U}{\partial Y^2} \tag{8}$$

$$\frac{\partial V}{\partial \tau}+U\frac{\partial V}{\partial X}+V\frac{\partial V}{\partial Y}=-\frac{\partial P}{\partial Y}+\frac{\partial^2 V}{\partial X^2}+\frac{\partial^2 V}{\partial Y^2} \tag{9}$$

$$\frac{\partial T}{\partial \tau}+U\frac{\partial T}{\partial X}+V\frac{\partial T}{\partial Y}=\frac{1}{\mathrm{Pr}}\left(\frac{\partial^2 T}{\partial X^2}+\frac{\partial^2 T}{\partial Y^2}\right) \tag{10}$$

with the initial and boundary conditions (5) in the dimensionless form as:

$$\begin{aligned}
&\tau=0\text{: } 0\le X\le 1, 0\le Y\le 1, U=V=0, T=0\\
&\tau>0\text{: } X=0; \quad U=V=0; \quad \frac{\partial T}{\partial X}=0\\
&\qquad X=1; \quad U=V=0; \quad T=2Y-1\\
&\qquad Y=0; \quad U=V=0; \quad T=\begin{cases}1 & 0\le X\le 0.5\\ -1 & 0.5<X\le 1\end{cases}\\
&\qquad Y=1; \quad U=V=0; \quad T=\begin{cases}-1 & 0\le X\le 0.5\\ 1 & 0.5<X\le 1\end{cases}
\end{aligned} \tag{11}$$

By introducing dimensionless vorticity $\varsigma=-\nabla^2\psi$ in equations (7)-(9) the problem statement can be written as:

$$\frac{\partial \varsigma}{\partial \tau}+U\frac{\partial \varsigma}{\partial X}+V\frac{\partial \varsigma}{\partial Y}=\frac{Gr}{2}\frac{\partial T}{\partial y}+\nabla^2\varsigma \tag{12}$$

$$\frac{\partial T}{\partial \tau}+U\frac{\partial T}{\partial X}+V\frac{\partial T}{\partial Y}=\frac{1}{\mathrm{Pr}}\nabla^2 T \tag{13}$$

where the dimensionless stream function ψ is given by:

$$U=\frac{\partial \psi}{\partial Y} \text{ and } V=-\frac{\partial \psi}{\partial X} \tag{14}$$

The corresponding boundary conditions are:

$$\begin{aligned}
&\tau=0\text{: } 0\le X\le 1, 0\le Y\le 1, \varsigma=0, T=0\\
&\tau>0\text{: } X=0; \quad \psi=\frac{\partial \psi}{\partial X}=0; \quad \frac{\partial T}{\partial X}=0\\
&\qquad X=1; \quad \psi=\frac{\partial \psi}{\partial X}=0; \quad T=2Y-1\\
&\qquad Y=0; \quad \psi=\frac{\partial \psi}{\partial Y}=0; \quad T=\begin{cases}1 & 0\le X\le 0.5\\ -1 & 0.5<X\le 1\end{cases}\\
&\qquad Y=1; \quad \psi=\frac{\partial \psi}{\partial Y}=0; \quad T=\begin{cases}-1 & 0\le X\le 0.5\\ 1 & 0.5<X\le 1\end{cases}
\end{aligned} \tag{15}$$

After obtaining the values of T, the local Nusselt number, Nu, $(= (\partial T/\partial Y)_{Y=0})$ and its mean value, $\overline{Nu}$, over the height of the enclosure are calculated based on Gr, Pr, l and τ.

3. Method of solution

The system of unsteady coupled nonlinear partial differential equations (12) and (13) is solved by finite-difference technique as explained below. If a solution for ζ and T fields are found at $\tau = n\Delta\tau$ (where $n = 0$ corresponds to the initial condition) then the solution at the next time level $(\tau = (n+1)\Delta\tau)$ is calculated by employing alternate direction implicit (ADI) method. The vorticity and energy equations (12) and (13) are transferred into a tridiagonal system of equations which is solved by Thomas algorithm. An added advantage of using ADI method is that larger time increments can be incorporated in solving the system of equations without loss of stability. It is also shown (elsewhere) that this method is stable for any ratio of time increments to space increments as long as the same time increment is kept at all levels.

After calculating the temperature and interior vorticity at an advanced point of time, the stream function is then calculated by using the successive over relaxation method. Velocity components and boundary vorticity are obtained from these values of stream function. The vorticity values at the corners are taken as averages of the values of vorticity at the two neighboring nodes. This sequence beginning with the ADI solution of the energy equation is applied repeatedly until the desired results are acquired. The convergence criteria used for the field variables $\phi = (T, \varsigma, \psi)$ is given by:

$$\frac{\phi_{n+1}(i,j) - \phi_n(i,j)}{\phi_{n+1}(i,j)} \leq 10^{-5},$$

where the index n represents the iteration number. Time increment of 0.001 is taken in all the calculations.

The numerical results presented in this paper are estimated from a 41×41 grid system. Figure 2 shows $\overline{Nu}$ values obtained for different grid systems, namely, 21×21 to 81×81. From this figure it can be observed that after 41×41 grid system, there is not considerable change in the values of $\overline{Nu}$, when the grid size is increased further. Therefore, the 41×41 grid is used in the present study.

Prior to the computational calculations, as a partial verification of the computational procedure, the $\overline{Nu}$ and ψ_m (stream function at the cavity mid point) results for different Ra and Pr were compared with the steady-state solutions given by Wilkes and Churchill (1966) and De Vahl Davis (1968). Wilkes and Churchill (1966) and

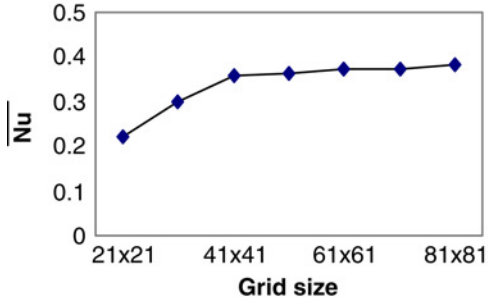

Figure 2.
Effect of grid system size on $\overline{Nu}$ at Gr = 20,000

De Vahl Davis (1968) considered a square enclosure with one vertical wall heated and the other cooled along with linear and insulated boundary conditions on the horizontal walls. The results are tabulated in Tables I and II for comparison.

4. Results and discussion

The flow structure usually depends on the geometrical parameters (X and Y) and the control parameters *Gr* and *Pr*. In the present work, the effect of *Gr* is studied by keeping the geometrical parameters and the control parameter $Pr = 0.733$ (air) fixed. The computations were started at $Gr = 100$. At this low *Gr*, the simulated flow field was observed to be steady and laminar. When *Gr* was increased, the flow was observed to transit from one equilibrium state to another due to the presence of rapidly varying disturbance field. The flow remained steady until $Gr < 20{,}900$. At slightly increasing Grashof number to $Gr = 20{,}900$, the flow, however, started to exhibit a time-periodic solution.

Figure 3 shows the velocity U at an arbitrarily chosen location (0.75, 0.75) inside the cavity for *Gr* ranging from 5,000 to 30,000. The velocity *U* is observed to be steady for values of *Gr* up to 20,900. When $Gr > 20{,}900$, the bifurcation diagram depicted in this figure shows the existence of two solutions for the stream wise velocity component U. The computational results signify that for $Gr < 20{,}900$, the flow remains steady and laminar and further increase in the *Gr* values leads to time periodic solution. The transitional flow leading to oscillatory flow occurs at $Gr = 20{,}900$.

Figure 4 illustrates the simulated streamlines and isotherms at $Gr = 100$. From Figure 4(b) it can be seen that the flow field in the cavity is characterized by the presence of two counter-rotating cells, with the cell near the top left corner of the cavity rotating clockwise and the cell near the bottom right corner rotating counter-clockwise. Fluid in contact with the heated side of the cavity shows a tendency to rise due to the decrease in fluid density and starts to move towards the cooled portion of the cavity. The temperature difference in the cavity along both horizontal and vertical directions leads to the formation of the counter rotating cells. In Figure 4(a), the simulated isotherms of the flow field clearly show that the energy transport in the cavity is

Table I. Comparison of average Nusselt number and stream function values at the cavity midpoint

Ra	*Pr*	Parameter	De Vahl Davis (1968)	Present study
10,000	0.733	$\overline{Nu}$	1.773	1.704
		ψ_m	6.429	6.214
10,000	10.0	$\overline{Nu}$	1.769	1.74
100	0.733	ψ_m	0.1582	0.12
1,000	0.733	ψ_m	1.54163	1.5

Note: ψ_m – Stream function at the cavity mid point

Table II. Comparison of average Nusselt number

Boundary condition	*Gr*	*Pr*	$\overline{Nu}$ Wilkes and Churchill (1966)	Present study
Linear	6,850	0.733	1.419	1.624
Linear	20,000	0.733	2.068	2.280
Insulated	20,000	0.733	2.874	2.612

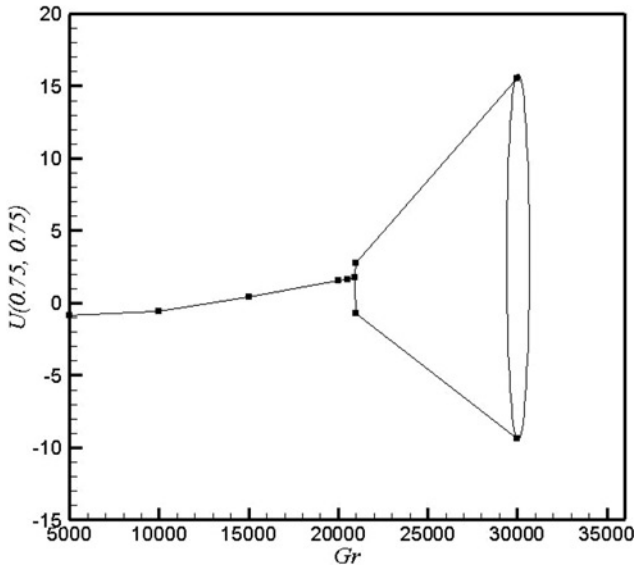

Figure 3.
The bifurcation diagram at the arbitrarily chosen location (0.75, 0.75)

governed primarily by conduction. Also, the steady-state stream function values $\psi_{max} = 0.022$ and $\psi_{min} = -0.014$ obtained at $Gr = 100$ indicate the prevalence of conduction. Major portion of the cavity is occupied by the slow moving fluid.

Figure 5 illustrates the simulated steady-state isotherm contours and stream lines obtained at different values of *Gr*. A significant change in the isotherm pattern is seen at $Gr = 20{,}500$ compared to $Gr = 10{,}000$. The isotherms show a gradual departure from the conduction dominated pattern shown in Figure 4(a) and are observed to be more concentrated near the vertical walls. A more uniform temperature distribution is seen at the center of the cavity. Fluid along the hot portion of the walls gets heated up and move towards the cooler portion to form two counter rotating cells. Values of the stream function increases as *Gr* increases, shows the acceleration of the fluid.

To study the effect of *Gr* on the temperature *T* and velocity *U*, simulations of the flow were performed at $Gr = 5{,}000$, 10,000, 20,000, 30,000 and 40,000. Figure 6 shows the effect of *Gr* on the temperature T with respect to Y at $X = 0.5$. The temperature is steady and rises very rapidly near the walls compared to other locations irrespective of *Gr*. Figure 7 exhibits the unsteady behavior of T at $Gr = 21{,}000$. Time evolution of temperature at three different locations (0.75, 0.75), (0.5, 0.5) and (0.25, 0.75) inside the cavity are shown. The inset figure clearly illustrates the oscillations in the temperature. It can be observed that oscillation of T at the center of the cavity (0.5, 0.5) is less compared to other locations. Temperature calculations at all these three different locations show thermal instability.

Mid height velocity U (0.5, Y) profiles at different *Gr* are shown in Figure 8. At $Gr = 5{,}000$, heat transfer is mainly by conduction and hence very minimum changes occurred in *U* values. When *Gr* increases further, convective effects become stronger to cause steep increase in *U* values. Velocity U is found to reach maximum near the center of the cavity. Figure 9 shows time evolution of *U* at three different locations (0.5, 0.5), (0.75, 0.25) and (0.25, 0.75) at $Gr = 21{,}000$. The inset figure clearly exhibits the

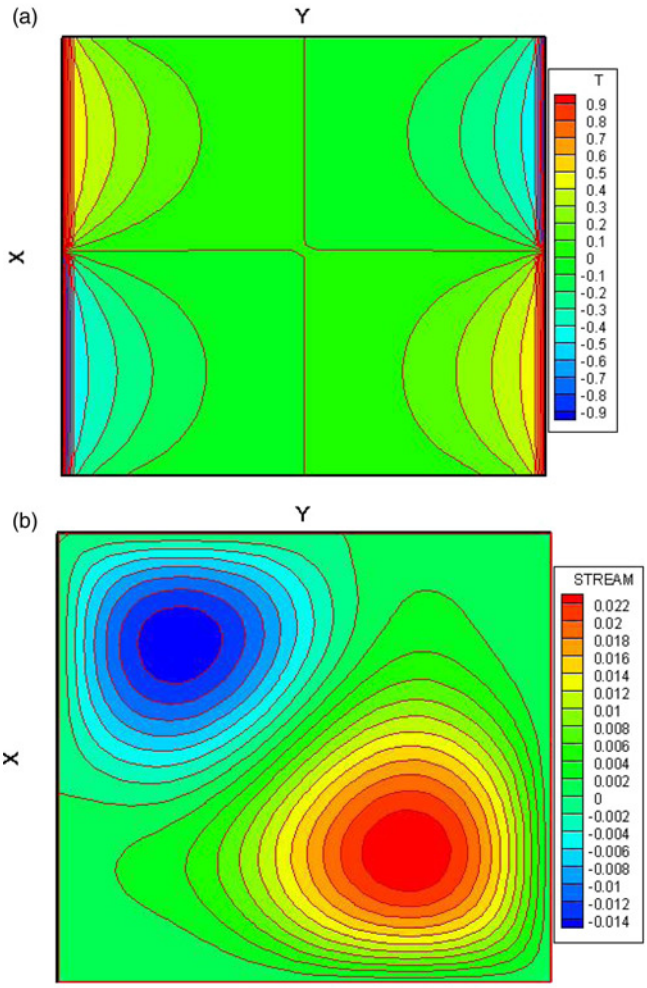

Figure 4.

Notes: (a) Steady-state isotherms at $Gr = 100$ and (b) steady-state stream lines at $Gr = 100$

unsteady behavior of U. At (0.5, 0.5) though velocity is maximum, oscillations are observed to be minimum compared to other two locations. Velocity estimation at these three locations exhibits unstable nature.

Figure 10 shows the unsteady behavior of average Nusselt number at $Gr = 21{,}000$. The inset figure shows the oscillations of $\overline{Nu}$. The unsteady nature of $\overline{Nu}$ is due to the increasing oscillations in the temperature values.

Figure 11 shows the stream function and isotherm contours at $t = 9.0000$ and $t = 9.0004$ when $Gr = 30{,}000$. A significant change in the isotherm pattern is observed in Figures 11(a) and (b). Distinctly different pattern of counter rotating cells is seen in Figures 11(c) and (d).

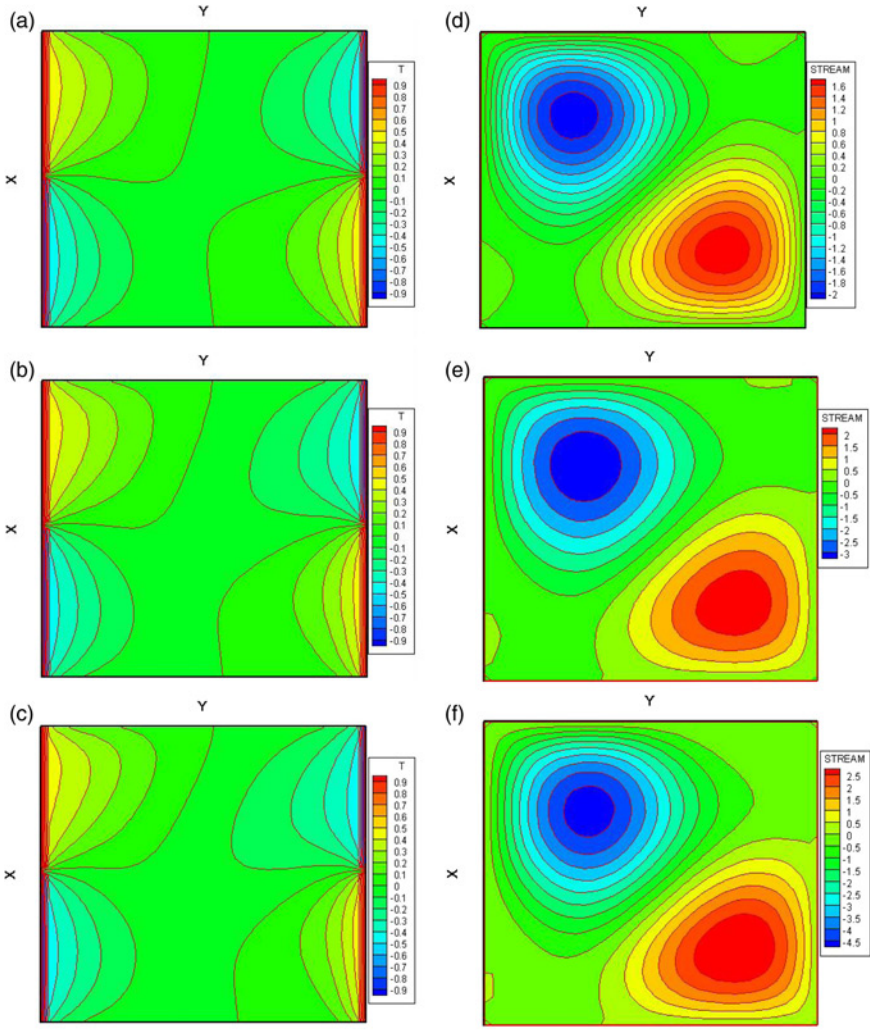

Notes: Steady-state isotherms at (a) Gr = 10,000, (b) Gr = 15,000, (c) Gr = 20,500 and steady-state stream lines at (d) Gr = 10,000, (e) Gr = 15,000, (f) Gr = 20,500

Figure 5.

At $t = 9.0$, a clockwise rotating cell develops and occupies the major portion of the cavity and a small counter clockwise rotating cell is seen near the bottom right corner. At $t = 9.004$, this counter clockwise rotating cell grows in size and suppresses the clockwise rotating cell. Significant part of the cavity has fluid with large temperature gradients which results in visibly dominant rotating cell. More oscillations seen in the velocity values, when Gr is increased further, finally leads to unsteady behavior.

Amplitude of the fluctuations in the computed quantities grows as Gr increases further is shown in temperature T and velocity U values (see Figures 12 and 13) at the arbitrarily selected location (0.5, 0.5) inside the cavity at $Gr = 100{,}000$. Time periodic behavior is observed.

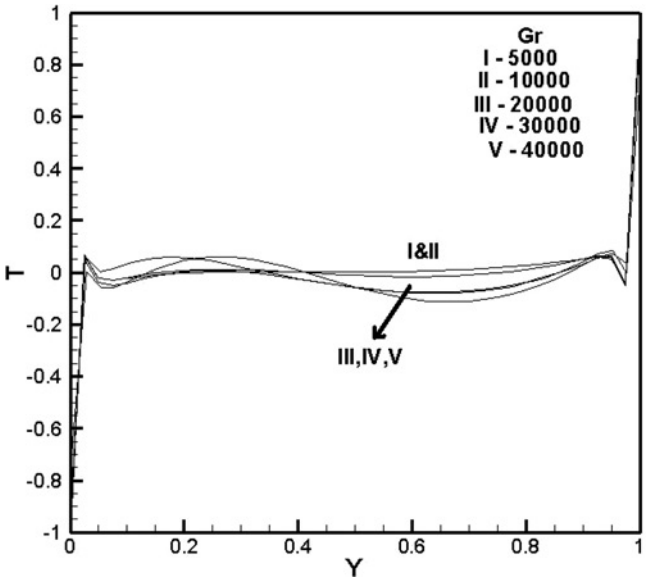

Figure 6.
Mid-height temperature profiles at different *Gr* values

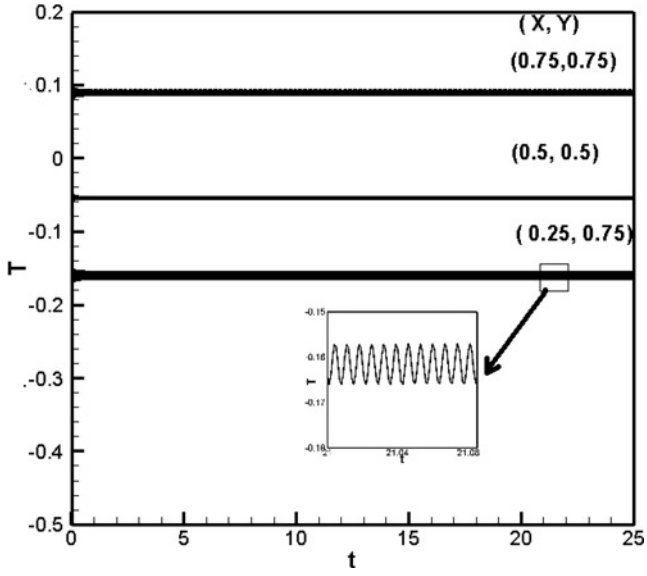

Figure 7.
Temperature T at three different locations at $Gr = 21{,}000$

5. Conclusion

Numerical predictions of unsteady natural convection flow in a square cavity with partially heated and cooled vertical walls, adiabatic top wall and linearly heated bottom wall have been presented. The non-dimensional governing equations were solved numerically by the ADI finite difference method. From the simulations of the flow performed over the range of Grashof number from 100 to 30,000, the flow pattern was

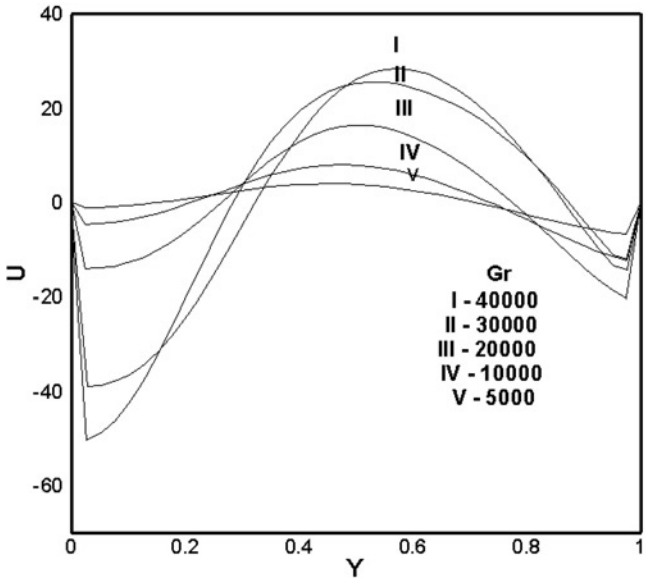

Figure 8.
Velocity U at (0.5, Y) at different Gr

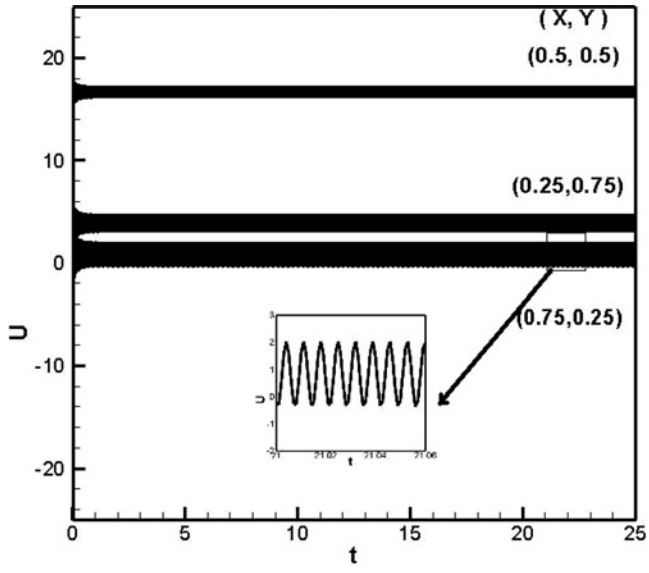

Figure 9.
Velocity U at three different locations when $Gr = 21{,}000$

found to depend on the Gr value. At low values of Gr, energy transport in the cavity was mainly by conduction. Flow pattern changes occurring with increasing Gr were analyzed with the aid of streamlines, isotherms and average Nusselt number. On increasing Gr, stream function values increased considerably due to the change in heat transfer mode from conduction to convection. The flow was found to be steady and laminar for $Gr < 20{,}900$ and oscillatory for $Gr > 20{,}900$. Oscillations in the temperature,

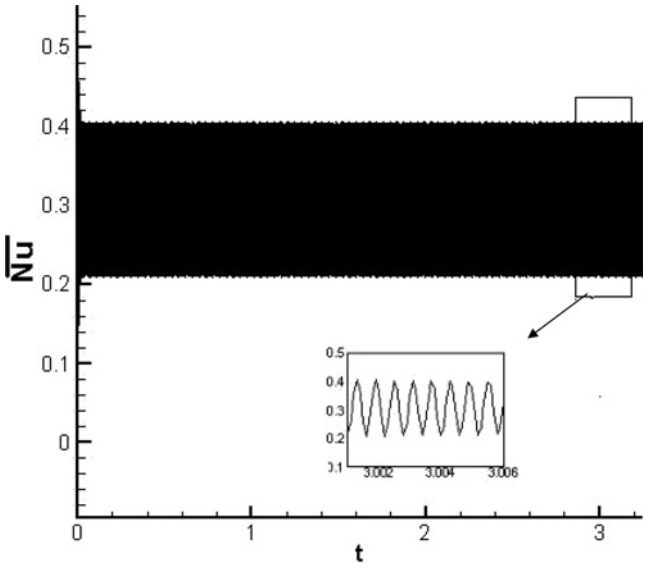

Figure 10.
Average Nusselt number vs time at $Gr = 21{,}000$

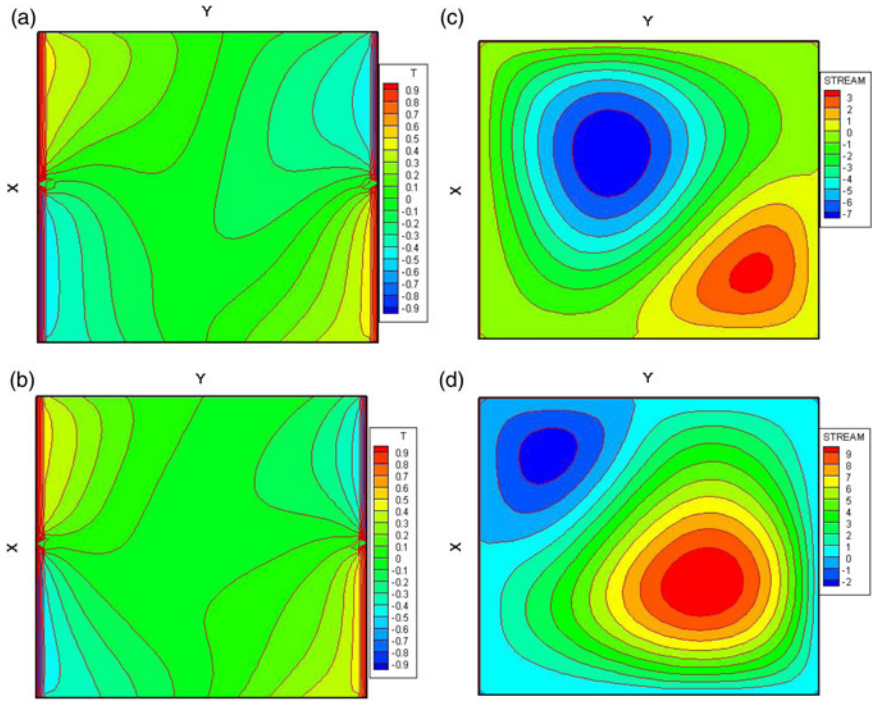

Figure 11.

Notes: Unsteady-state isotherms at (a) t = 9.0000 and (b) t = 9.0004 when $Gr = 30{,}000$, and unsteady-state stream lines at (c) t = 9.0000 and (d) t = 9.0004 when $Gr = 30{,}000$

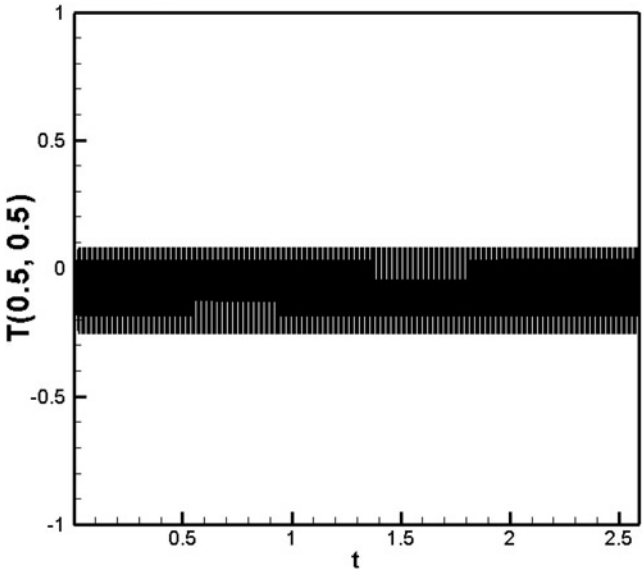

Figure 12.
Temperature T at the location (0.5, 0.5) inside the cavity at $Gr = 100{,}000$

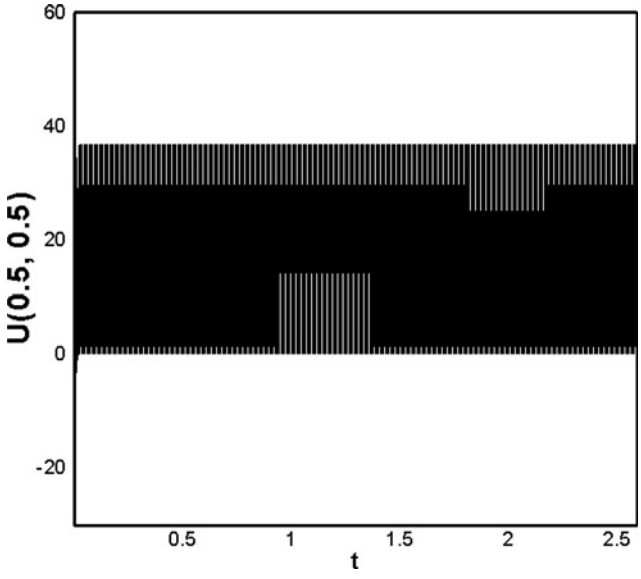

Figure 13.
Velocity U at the location (0.5, 0.5) inside the cavity at $Gr = 100{,}000$

velocity and average Nusselt number were calculated at $Gr = 21{,}000$ and $Gr = 30{,}000$. The amplitude of the fluctuations in T, U and $\overline{Nu}$ were found to increase considerably on increasing Gr. Signs of change, in the flow pattern, began at $Gr = 20{,}900$ and on further increasing Gr the flow became unsteady. The analysis of the results revealed that the flow field was appreciably influenced by the Grashof number.

References

Basak, T., Roy, S. and Balakrishnan, A.R. (2006), "Effects of thermal boundary conditions on natural convection flows within a square cavity", *International Journal of Heat and Mass Transfer*, Vol. 49, pp. 4525-35.

De Vahl Davis, G. (1968), "Laminar natural convection in an enclosed rectangular cavity", *International Journal of Heat and Mass Transfer*, Vol. 11, pp. 1675-93.

Kandaswamy, P. and Nithyadevi, M. (2007), "Buoyancy driven convection of water near its density maximum with partially active vertical walls", *International Journal of Heat and Mass Transfer*, Vol. 50, pp. 942-8.

Marcello, M.G. and Milanez, L.F. (1995), "Natural convection in rectangular enclosures heated from below and symmetrically cooled from the sides", *International Journal of Heat and Mass Transfer*, Vol. 38, pp. 1063-73.

Newell, M.E. and Schmidt, F.W. (1970), "Heat transfer by laminar natural convection within rectangular enclosures", *ASME Journal of Heat Transfer*, Vol. 11, pp. 159-68.

Sathiyamoorthy, M., Basak, T., Roy, S. and Pop, I. (2007), "Steady natural convection flows in a square cavity with linearly heated side walls", *International Journal of Heat and Mass Transfer*, Vol. 50, pp. 766-75.

Valencia, A. and Fredrick, R.C. (1989), "Heat transfer in square cavities with partially active vertical walls", *International Journal of Heat and Mass Transfer*, Vol. 32, pp. 1567-74.

Wilkes, J.O. and Churchill, S.W. (1966), "The finite difference computation of natural convection in a rectangular enclosure", *A.I.Ch.E. Journal*, Vol. 12, pp. 161-6.

Wright, J.L., Jin, H., Holland, K.G.T. and Naylor, D. (2005), "Flow visualization of natural convection in a tall, air-filled vertical cavity", *International Journal of Heat and Mass Transfer*, Vol. 49, pp. 889-904.

Wu, W., Ewing, D. and Ching, C.Y. (2005), "The effect of top and bottom wall temperatures on the laminar natural convection in an air-filled cavity", *International Journal of Heat and Mass Transfer*, Vol. 49, pp. 1999-2008.

Yang, K.T. (1988), "Transition and bifurcations in laminar buoyant flows in confined enclosures", *Transactions of ASME – Journal of Heat Transfer*, Vol. 110, pp. 1191-8.

Further reading

Batchelor, G.K. (1967), *An Introduction to Fluid Dynamics*, Cambridge University Press, Cambridge.

Larroude, P.H., Ouazzani, J., Alexander, J.I.D. and Bontoux, P. (1994), "Symmetry-breaking flow and oscillatory flows in a 2D directional solidification model", *European Journal of Mechanics – B/Fluids*, Vol. 13 No. 3, pp. 353-8.

About the authors

Rangaswamy Navamani is a Selection Grade Lecturer. He has 20 years of teaching experience and presented 12 papers at national and international conferences. Rangaswamy Navamani is the corresponding author and can be contacted at: rnavamani66@yahoo.co.in

Nadarajan Murugan is a Professor. He has 26 years of teaching and research experience and has published 48 papers in international journals and 135 papers at national and international conferences. He has guided 11 PhDs and received the Prestigious McKay-Helm Award for the best contribution for the advancement of knowledge in the field of stainless-steel surfacing from the American Welding Society for the year 1998.